Article

Flash Pyrolysis of Oleaginous Biomass in a Fluidized-bed Reactor

Brook Urban, Yaser Shirazi, Balakrishna Maddi, Sridhar Viamajala, and Sasidhar Varanasi

Energy Fuels, **Just Accepted Manuscript** • Publication Date (Web): 05 Jul 2017

Flash Pyrolysis of Oleaginous Biomass in a Fluidized-bed Reactor

Brook Urban [1], Yaser Shirazi [1], Balakrishna Maddi [1,2], Sridhar Viamajala [1*] and Sasidhar Varanasi[1]

[1] *Department of Chemical and Environmental Engineering, University of Toledo, Toledo OH 43606*

[2] *Pacific Northwest National Laboratory, Richland, WA 99354*

* Corresponding author

Email: sridhar.viamajala@utoledo.edu

Phone: 419-530-8094

Fax: 419-530-8086

Abstract

In this study, flash pyrolysis was performed using milled soybean as a model substrate to assess the production of liquid fuels from oleaginous biomass feedstocks. A laboratory-scale fluidized-bed flash pyrolysis reactor that allowed rapid heat transfer to the biomass along with short vapor residence time, was designed and constructed. Pyrolysis was performed between 250-610 °C with a vapor residence time between 0.2-0.3 s. At 550 °C or higher, nearly 70 % of the initial feed mass as well as feed carbon was recovered in bio-oil. In addition, 90 % of the feedstock lipids were recovered in the bio-oil at these pyrolysis conditions. The high liquid products yields were attributed to (1) the low secondary degradation of bio-oils due to the short vapor residence time and (2) the high recovery of liquids in a novel dry ice packed-bed condenser that provided a high surface area for condensation/aggregation of dilute bio-oil vapors/aerosols that were entrained in the carrier gas. The bio-oil from this study had higher C- and H- content, higher calorific value and lower oxygen and water content than bio-oil from wood. These results show that high-quality bio-oil at high yield can be obtained from flash pyrolysis of oleaginous feedstock.

Key words: Flash pyrolysis, Oleaginous biomass, Bio-oil, Lipid, Bio-char

1 Introduction

Production of liquid fuels from biomass is desirable due to the ease of transport and storage of the liquid along with the high energy density required for internal combustion engines.[1] Oleaginous feedstocks such as oilseeds and microalgae are attractive biomass resources for biofuel production due to presence of energy dense triglycerides and fatty acids.[2]

A common approach to produce liquid fuel from oleaginous feedstocks such as oilseeds or microalgae is through extraction of biomass lipids followed by transesterification. For oilseeds, lipids are typically recovered through a combination of mechanical operations such as pressing and grinding followed by solvent extraction. For edible oil seeds, the residual meal is usable for human or animal consumption. However, in the case of oil seeds such as jatropha and some members of the mustard and castor families, the oils and/or meal may be non-edible due to presence toxic hydroxy fatty acids, ricin and glucosinolates.[3, 4] In the US, some varieties of non-edible oil seed producing plants (e.g. pennycress and camelina) are being actively developed by the US Department of Agriculture as "off season rotation crops" that can be grown in rotation with traditional food crops.[5-8] For such biofuel feedstocks, it is desirable to convert all the seed material into fuel. But, when subjected to *a priori* lipid recovery, the residues must be separately processed to fuels using secondary biochemical or thermochemical methods. For dedicated fuel production from oleaginous feeds, it is likely more advantageous to produce fuels or fuel-precursors from the entire feedstock (for higher yields), rather than applying a first lipid extraction step.

In this context, thermochemical conversion such as pyrolysis and hydrothermal liquefaction, are potential one-step methods to process oleaginous feedstocks.[9-11] Typical reaction conditions for hydrothermal liquefaction are pressures between 50-200 atm and temperatures between 250-450 °C [10, 12, 13] and as a result, hydrothermal liquefaction can incur high capital cost. However, this approach remains attractive for processing oleaginous microalgae since these feedstocks are wet when harvested and conversion via hydrothermal liquefaction can avoid costs for drying. [13, 14]

A more preferable thermochemical approach for feedstocks that are substantially dry (e.g. oilseeds) is pyrolysis.[5, 15, 16] The major factors that control the yields of liquid (bio-oil), solid (char) or non-condensable gas products are temperature, heating rate, and vapor residence time.[17, 18] Pyrolysis performed at moderate temperatures (400-650 °C) together with short vapor residence times and fast heating rates promote higher bio-oil yields.[12, 19] Particularly high liquid yields are obtained during "flash pyrolysis" in fluidized-bed reactors that allow vapor residence times of less than 1 s.[20] The pyrolysis vapors that are removed along with the carrier gas are then quickly quenched/condensed to minimize thermal degradation of the liquid products to non-condensable gases.[12]

In this study, a fluidized-bed flash pyrolysis system was designed, constructed and used to assess the flash pyrolysis behavior of oleaginous materials. In addition to the reactor, the pyrolysis system was comprised of a series of conventional condensers followed by a novel "packed-bed condenser" that comprised of a column packed with crushed dry ice. The large inert surface area of the packed-bed condenser allowed for efficient capture of bio-oil aerosols; the bio-oil was easily recovered after the dry ice vaporized. Soybean were used as a model feedstock since this oilseed has been well

characterized in the literature and also has similar characteristics (elemental composition, lipid content, and calorific value) as the non-edible pennycress [5]. Flash pyrolysis experiments were performed to assess optimum conditions for high-yield recovery of bio-oil. To our knowledge, this is the first study to report high bio-oil yield (70%) from flash pyrolysis of oleaginous feedstocks in a fluidized bed reactor.

2 Materials and methods

2.1 Materials

Organic soybean flakes were obtained from Shiloh Farms (New Holland, PA, USA). The soybean flakes were milled using an electric coffee grinder. The resulting particles were then sorted using sieve trays to an -18/+20 mesh size. This corresponds to a particle size between 8.4mm and 1mm. Hexane, chloroform, methanol, acetone and N-methyl-2-pyrolidone (NMP) were purchased from Fisher Scientific (Pittsburgh, PA, USA). Analytical standards for fatty acids (stearic acid, oleic acid, linoleic acid, and palmitic acid), oleamide, glycerides (triolein, diolein, and monolein), and alkanes (mixtures of C_7-C_{30}) were purchased from Sigma-Aldrich (St. Louis, MO, USA).

2.2 Thermodynamic properties of carrier gas

N_2 properties (density, viscosity, conductivity, specific heat capacity) at reactor temperature (250 °C-610 °C) and pressure (20 psia) were obtained from the NIST chemistry webbook.[21]

2.3 Experimental set-up

The schematic diagram of the experimental set-up is shown in Figure 1 and a scaled drawing of the fluidized bed reactor is shown in Figure S1 (supplementary

information). The experimental apparatus consisted of feed, reactor and condenser sections.

2.3.1 Feed section

The feed section consisted of a feed hopper connected to a venturi that allowed introduction of feed particles into the reactor due to suction created by the carrier gas (N_2) moving upward through the venturi (see "feed section" box in Figure 1). The absence of mechanical moving parts during feed transfer minimized the chance of biomass attrition and feed-port plugging. The length of the venturi (from the start of the inlet curve to the end of the outlet curve) was 4″ (shown in Figure S2, supplementary information). The inlet diameter (d_1) and throat diameter (d_2) were 1.05″ and 0.25″, respectively, and are consistent with Levenspiel's recommendation of $d_2 \leq \frac{d_1}{4}$ for a well-designed venturi.[22] d_2 was set to 0.25″ to keep the throat diameter slightly larger than the inlet orifice (0.24″) receiving biomass from the feed hopper (see labels for inlet orifice in Figure S2, supplementary information). The venturi throat was 0.47″ long and was designed to maintain a high gas velocity for sufficient distance and prevent accumulation of biomass (and possibly plugging) at the throat orifice. For venturi-based flow rate measurement devices (such as the venturi meter), the throat lengths are shorter and usually equal to one throat diameter.[23]

The length of the inlet section of the venturi (from the start of the reducer to the throat, Figure S2, supplementary information) was 0.8″. This resulted in an entrance cone angle of 26° and is close to the angle of 21°± 2° considered as optimum.[23] The length of the outlet section was 2.7″. This gave the outlet cone angle of 8.4° and is within the

recommended range of 5-15° for the exit cone angle.[23] Larger cone angles could cause streamline separation from the walls creating eddies and additional pressure drop.

The feed hopper was pressurized using N_2 gas and attached to the venturi by means of a 0.24″ OD tube. The hopper had a clear cap that was fitted with an inlet for N_2 gas (for purging and pressurizing the hopper) and a pressure gauge. A block valve placed at the exit of the hopper chamber, prevented premature transfer of feed into the reactor prior to start of the experiment.

2.3.2 Reactor section

The feed unit was connected to a reactor section for fluidization and pyrolysis of the feed particles (see "reactor section" box in Figure 1). The reactor section consisted of a primary reactor tube connected to a larger diameter disengagement chamber via a short expander. The reactor tube was designed to be 1.05″ ID and 10″ long from the venturi exit to the inlet of the expander. The expander was a truncated cone of 4.89″ length with an angle of 11°. This slope allowed smooth transition of flow between the unequal-diameter reactor and disengagement tubes. The diameter of the disengagement chamber was 3″ and height 6″. All dimensions are shown in Figure S1 (supplementary information). The larger diameter disengagement chamber was added to decrease the carrier gas velocity to below the terminal velocity of the biomass particles such that they were no longer entrained in the carrier gas and could stay within the reactor. Attached to the top end of the disengagement chamber was a flanged cap that was removable for cleaning the reactor between experiments. Two K-type thermocouples were inserted into the reactor through the top cap to monitor temperature during pyrolysis. One measured the temperature at the exit of the venturi while the other measured the temperature in the

disengagement chamber immediately after the expander section. These were attached to Omega temperature controllers for data recording. An additional thermocouple monitored the furnace temperature.

Reactor internal pressure was measured using a pressure gauge connected to a 1/8″ OD stainless steel tube that was inserted into the reactor through the top cap. The internal end of the tube was bent at a 90° angle to prevent plugging due to biomass or bio-oil. The length of tubing exiting the reactor was approximately 2′ in length and coiled to cool the tube and prevent damage to the pressure gauge from heat. Since the pressure gauge was sealed, the measurement indicated pressure of stagnant gas inside the tubing and thereby, pressure in the reactor.

The reactor was placed within two clamshell furnaces (Applied Test Systems Inc, Butler, PA, USA) placed on top of each other (see reactor assembly photograph in Figure S3, supplementary information) and the carrier gas tube (1/8″ OD and 3′ long) was coiled around the reactor to allow preheating of the carrier gas before it entered the reactor. Inlet flow rate of the carrier gas was controlled by a variable area flow meter.

2.3.3 Condenser section

The condenser section consisted of two glass Allihn condensers that were connected in series followed by a dry ice packed-bed condenser (see "condenser section" box in Figure 1). The utility fluid used in the Allihn condensers was a mixture of propylene glycol and acetone that was cooled by dry ice. The cold utility fluid was pumped through the glass condenser series in a countercurrent flow mode.

The packed-bed condenser was made of a glass tube – 3.5" diameter and 3′ length (see photograph in Figure S4, supplementary information). The packing was a mixture of

different sized crushed dry ice. The bottom 4" of the condenser was packed loosely with large 1-2″ chunks of dry ice. Then finely powdered dry ice was added for an additional height of 4″. This alternating pattern of coarse and fine dry ice was repeated until the glass tube was full. The dry ice packed-bed condenser technique creates an extremely large and cold surface area for the vapors to condense. . At the end of the experiment, the dry ice evaporates, allowing all of the condensed oils to drop to the bottom of the condenser for easy recovery. At laboratory scale, the dry ice packed-bed condenser technique maximizes bio-oil recovery and allows accurate assessment of the bio-oil yields and compositions.

Liquid traps were placed at the bottom of the packed-bed condenser and the Allihn condenser to collect liquid products. Liquids adhered to the condenser walls were recovered with a home-made squeegee.

2.4 Experimental procedure

Pyrolysis reactions were performed at temperatures ranging from 250 °C to 610 °C. For each experiment, 30 g of oven-dried biomass was used as feed, and the inlet flow rate of carrier gas was maintained at 0.375 ft^3/min at an inlet pressure of 110 psia.

Prior to each experiment, the furnaces were set to 600 °C to vaporize any previous residue from the reactor while an N_2 purge was maintained to carry away any vapors that were generated. After approximately 1h, the set points of the reactor furnace were lowered to the desired reaction temperature. As the reactor and furnace equilibrated to the desired reaction temperature, the hopper was loaded with biomass then sealed and purged with N_2. Once the reactor and furnaces were equilibrated to the desired reaction temperatures (based on the internal and furnace thermocouples), the condenser series was

connected to the reactor outlet and cold utility flow was started. The carrier gas flow rate was maintained until the reactor and condensers were fully equilibrated. To start the experiment, the hopper pressure was increased and the block valve on the feed hopper was slowly opened to allow the biomass feed to be introduced to the reactor.

After the reaction was completed, the reactor furnaces were turned off, the carrier gas flow was stopped and the utility fluid was drained from the Allihn condensers. The bio-oil was then recovered from the condensers, traps and tubing. The bio-oil in the packed-bed condenser was recovered after the dry ice evaporated. All of the recovered bio-oil was pooled in to a vial and weighed on an analytical balance (Mettler Toledo, USA) with ± 0.1 mg accuracy. Depending upon the pyrolysis temperature, the recovered liquid was comprised of a single phase or two separate phases. When two phases were present, the liquid products were separated into aqueous- and oil- phases using a separatory funnel. Thereafter, the oil and aqueous phases were placed into separate vials and weighed. The solid residues (bio-char) were also removed from the reactor and weighed.

The yield of pyrolysis products relative to feed mass was calculated as

$$Y_{\text{Oil phase}} = \frac{W_{\text{Oil phase}}}{W_{\text{Biomass}}} \times 100 \quad (1)$$

$$Y_{\text{Aq. phase}} = \frac{W_{\text{Aq. phase}}}{W_{\text{Biomass}}} \times 100 \quad (2)$$

$$Y_{\text{Bio-char}} = \frac{W_{\text{Bio-char}}}{W_{\text{Biomass}}} \times 100 \quad (3)$$

$$Y_{\text{Bio-oil}} = Y_{\text{Oil phase}} + Y_{\text{Aq. phase}} \quad (4)$$

$$Y_{\text{Gas}} = 100 - (Y_{\text{Liq}} + Y_{\text{Bio-char}}) \quad (5)$$

where $W_{\text{Oil phase}}$, W_{Biomass}, $W_{\text{Aq. phase}}$, $W_{\text{Bio-char}}$ and $W_{\text{Bio-oil}}$ are the weights of oil phase, feed biomass, aqueous phase, bio-char and bio-oil, respectively.

2.5 Analytical methods

2.5.1 Feedstock characterization

Proximate analysis was carried out on oven dried biomass (105 °C for 12 h) to measure volatile matter, fixed carbon and ash content of biomass. Volatile matter content was determined with a thermo-gravimetric analyzer (SDT Q600 series analyzer, TA Instruments, Schaumburg, IL) by measuring weight loss after heating biomass samples from room temperature to 575 °C (temperature ramp rate of 10 °C/min) and holding for 7 min under N_2 atmosphere. Ash content (f_{ash}) was measured by heating biomass samples at 575 °C for 24 h to constant weight in a muffle furnace. The fixed carbon fraction was calculated by subtracting the volatile matter and ash (in percentage) from 100. Ultimate analysis was performed to measure elemental composition of biomass (see *Section 2.5.2.3*).

The Bligh and Dyer method used to measure the lipid content (f_{lipid}) of biomass.[24] Protein content ($f_{protein}$) was estimated by multiplying elemental nitrogen content by a factor of 6.25.[25] The carbohydrates mass fraction (f_{carb}) was estimated by Equation 6.

$$f_{carb} = 100 - f_{lipid} - f_{protein} - f_{ash} \quad (6)$$

2.5.2 Analysis of the pyrolysis products

2.5.2.1 Gas chromatography (GC) analysis

Chemical compounds in bio-oil were identified and quantified using a gas chromatograph (Shimadzu 2012 plus) equipped with a flame ionization detector (FID) and an auto sampler (AOC-20i). A RTX-biodiesel (Restek, Bellefonte, PA, USA) column was employed (15 m length, 0.32 mm ID, and 0.1 μm film thickness). The injector and detector temperatures were 370 °C. H_2 was used as the carrier gas with a flowrate of 6.02 mL/min and a split ratio of 1:10. The column temperature was initially set at 60 °C for 1 min, and was subsequently heated at a temperature ramp rate of 10 °C/min to 370 °C; this final temperature was maintained for 5 min at the end of the run. All chemical concentrations were estimated based on calibration curves developed using corresponding external analytical standards. All samples were analyzed three times and the mean value is reported.

GC-MS (Bruker, 450-GC equipped with 300-MS) analysis was performed to identify the chemical compounds in the pyrolysis products. An Agilent DB-5MS fused silica capillary column (length: 30 m, ID: 0.25 mm, and film thickness: 0.25 μm; Agilent Technologies, Santa Clara, CA) was used. The injector temperature was held constant at 300 °C and a split ratio of 1:100 was maintained during each sample analysis. Helium was used as carrier gas with constant column flow of 1.0 mL/min. The column was programed as follows: constant temperature of 30 °C for 10 min, followed by a temperature ramp 10 °C/min to 300 °C and a final hold for 10min. The transfer line, ion source, and manifold were maintained at 300 °C, 150 °C, and 40 °C, respectively. Chemical compounds corresponding to chromatogram peaks were identified using

NIST2008 mass spectral database. A minimum 70 % confidence level was used as a threshold for positive identification of IDs provided by the spectral analysis software.

The GC analysis used to specifically measure the concentration of fatty acids and glycerides in the bio-oil. GC-MS was used first to identify the fatty acids and glycerides in the bio-oil. Then, standard calibration curves were developed on the GC-FID for the chemical compounds that were identified by GC-MS. Finally, the bio-oils were analyzed on GC-FID, where the fatty acids and glycerides in the bio-oil were identified by matching the standards' retention time and quantified using corresponding standards' calibration curves. Prior to analysis, bio-oil samples were homogenized and diluted with 1 mL of a solvent – 1-methyl-2-pyrrolidone for GC-FID and acetone for GC-MS.

2.5.2.2 Water content of liquid products

Water content in the oil and aqueous phases was quantified using a Mettler Toledo V30 Volumetric Karl Fischer Titrator. The Ketone method or program was used for the analysis. The ketone method used a Hydranol-Medium K solvent along with Hydranol-Composite 5K as the titrant to avoid interference from aldehydes and ketones present in the bio-oil samples. The end drift was set at 25 μL/min.

2.5.2.3 Elemental analysis

Elemental analysis was performed using a Thermo Scientific Flash 2000 Organic Elemental Analyzer equipped with an auto-sampler to measure C, H and N. Both solid (biomass and bio-char) and liquid (oil and aqueous phases) samples were analyzed for C, H, and N content.

2.5.2.4 Calorific value

The higher heating values (HHV) of the biomass and bio-oils were calculated using previously established (Equations 7 and 8) ordinary least square (OLS) or partial least square (PLS) interpolation of experimentally measured calorific values of several fuels.[26] The HHV were assessed as the average of the OLS and PLS values, since previous studies have shown that estimates of HHV obtained as this average correspond well to experimentally measured HHV.[26]

$$HHV_{OLS} = 1.87 \times C^2 - 144 \times C - 2820 \times H + 63.8 \times C \times H + 129 \times N + 20147 \quad (7)$$

$$HHV_{PLS} = 5.22 \times C^2 - 319 \times C - 1647 \times H + 38.6 \times C \times H + 133 \times N + 21028 \quad (8)$$

where, C, H and N represent the mass fractions (within the range of 0-100) of elemental carbon, hydrogen and nitrogen within the sample and the HHV is in kJ/kg. Since elemental analysis also measures H in H_2O, the combustible H-content of bio-oil was calculated from difference of H that was measured from CHN analysis and from Karl Fisher Titration (H_2O consists of 11 wt. % H).

3 Results and discussion

3.1 Feedstock characterization

Table 1 shows the results of compositional, proximate and ultimate analysis of soybean flake used in the reported experiments. For later comparison of bio-oil yield and properties (Sections 3.3 and 3.4), composition data for other biomass feedstocks – a terrestrial biomass feedstock (woodchips) and a microalga (*Chlorella vulgaris*), are also shown. The data for woodchips were taken from our previous study[27] and data for *Chlorella vulgaris* were taken from the literature.[15] The compositional analysis of soybean flake and *Chlorella vulgaris* shows approximately similar content of

carbohydrate and protein. Also, the proximate analysis of soybean flake and *Chlorella vulgaris* indicates nearly similar volatile matter and fixed carbon, but lower ash. Low ash content in soybean flake is advantageous since inorganic elements in the ash are known to catalyze char formation during pyrolysis.[28] Elemental composition of soybean flake shows higher carbon content than *Chlorella vulgaris*, likely due to higher lipid content.

Woodchips had a much higher carbohydrate content than soybean flakes or microalgae and also contain lignin, rather than lipid but the C and H content of woodchips and soybean flakes were similar. Woodchips also show proximate compositions similar to soybean flakes. However, soybean flakes show much higher N content due to protein and less O due to lower carbohydrates.

3.2 Heat transfer and fluidization characteristics of the pyrolysis reactor

As discussed below, the physical design of the reactor system together with the operating conditions served the following objectives. First, the relatively high fluidization velocity allowed the maintenance of low vapor residence time to minimize secondary vapor-phase reactions and maximize liquid product yield. Second, the larger diameter (3″) disengaging section prevented entrainment and loss of biomass particles that often lead to inaccurate mass balances and overestimate of bio-oil yields when particles are carried over into condensers. Third, the smaller diameter reactor section allowed the biomass particles to remain fluidized such that heat transfer was rapid and uniform. Finally, the dry ice packed bed condenser ensured high recovery of the produced bio-oil. Due to the high carrier gas flow rates in fluidized bed reactors, bio-oil vapors form dilute aerosols upon cooling which are difficult to coalesce and recover by traditional heat exchange condensers. The dry ice condenser provided high surface area for inertial

impaction of these aerosols and also allowed easy recovery of bio-oils after natural evaporation of the dry ice at the end of the experiments.

The vapor residence time was calculated based on the fluidizing gas flow rates and reactor volume according to Equation (9)

$$\tau_{vap} = \frac{V\rho_g}{\dot{m}} \quad (9)$$

where, V is the volume of the reactor, ρ_g is the density of carrier gas (N_2) inside the reactor and $\dot{m}$ is the carrier gas mass flow rate. V was estimated from reactor dimensions and geometry (see Figure S1 and Section 2.2.2) to be 1.114 L. $\dot{m}$ was estimated from inlet carrier gas properties using Equation (10)

$$\dot{m} = \frac{P_i \dot{V}_i M}{RT_i} \quad (10)$$

where, P_i is the inlet carrier gas pressure (110 psia), $\dot{V}_i$ is the inlet carrier gas flow rate (0.375 ft^3/min), M is the molecular weight of N_2, R is the universal gas constant and T_i is the inlet gas temperature (20 °C). Since ρ varies with temperature, $\tau_{vap}$was also a function of temperature as shown in Figure S5 (supplementary information). Overall, τ_{vap} varied between 0.2 s and 0.32 s in the reported experiments (250 °C-610 °C). Due to the extremely short residence time, it is likely that secondary vapor-phase reactions were minimized.[12, 19, 20]

The heat transfer in the fluidized bed reactor used in this study occurred from the electrical furnaces around the reactor as well as from the preheated carrier gas. As such, the biomass particles received heat via convection from carrier gas as well as radiation from reactor walls. Heat transfer due to convection was assessed using the Ranz-Marshall correlation recommended for flow past spheres[29] and given as

$$\frac{h_c D_p}{k_g} = 2.0 + 0.60\left(Re_p\right)^{0.5}\left(\frac{c_{p,g}\mu_g}{k_g}\right)^{0.33} \quad (11)$$

where, h_c is the convective heat transfer coefficient, D_p is the diameter of the spherical particle (=8.4 mm), k_g is the thermal conductivity of the carrier gas, Re_p is the particle Reynolds number, $c_{p,g}$ is the specific heat capacity of the carrier gas at constant pressure, and μ_g is the dynamic viscosity of the carrier gas. Re_p is given as

$$Re_p = \frac{D_p G}{\mu_g} \quad (12)$$

where, G is the carrier gas mass velocity in the reactor section and was estimated by dividing $\dot{m}$ (Equation 10) with the cross sectional area (A) of the 1″ reactor section. Re_p decreased from a value of 190 to 133 while values of h_c increased from approximately 450 W/m^2·°C to 590 W/m^2·°C over the temperature range 250 °C-610 °C.

The radiation heat transfer coefficient for heat transfer to a particle at the time of its introduction into the reactor was determined by

$$h_r = \frac{q_r}{A(T_w - T)} = \frac{\sigma\varepsilon(T_w^4 - T^4)}{(T_w - T)} \approx \sigma\varepsilon T_w^3, when\ T_w \gg T \quad (13)$$

where, q_r/A is the heat flux by radiation, T_w is the temperature of the wall, T is the particle temperature, ε is the emissivity of the particle surface (=0.6[30]), σ is the Stefan-Boltzmann constant (=5.672×10^{-8} W/m^2·K^4). Over the temperature range of the experiments reported here, h_r values were much smaller than h_c (h_r/h_c<3%), and heat transfer due to radiation was deemed insignificant relative to convection.

To assess the relative importance of internal/external heat transfer rates and pyrolysis reaction kinetics, we estimated the Biot number (Bi) and Pyrolysis numbers (Py and Py') in our reactor as suggested by Pyle and Zaror.[31] These dimensionless quantities are defined in Equations 14-16 below.

$$Bi = \frac{h_c L}{k_p} \quad (14)$$

$$Py = \frac{k_p}{K \rho_p c_{p,p} L^2} \quad (15)$$

$$Py' = Bi \cdot Py = \frac{h_c}{K \rho_p c_{p,p} L} \quad (16)$$

where, L is the characteristic length ($= \frac{D_p}{6}$), k_p is the thermal conductivity of the particle (=0.116 W/m·K for soybean[32]), K is the apparent first order rate constant for the pyrolysis reaction which was estimated as a function of temperature by the Arrhenius equation using the activation energy and pre-exponential factors given by Pyle and Zaror,[31] ρ_p is the particle bulk density (=770 kg/m^3 for soybean[33]), and $c_{p,p}$ is the particle specific heat capacity (=1444 J/kg·K for soybean[34]). For the reactor temperatures used in this study, values of Bi were estimated to be between 0.5-0.7 indicating the presence of moderate internal temperature gradients. However, values of Py were >20 (i.e. $\gg$1) suggesting that the reactions proceeded slowly in comparison to the temperature wave. Finally, values of Py'were >15 (also $\gg$1) indicating that reaction kinetics, rather than external heat transfer controlled the rates of pyrolysis. Overall, these results indicate that product yields obtained in the fluidized bed reactor were a result of intrinsic pyrolysis kinetics rather than heat transfer limitations.

In addition to vapor residence time and reaction temperature, biomass heating rate is also an important parameter to consider, especially for defining the pyrolysis regime as slow, fast or flash.[17, 18] Heating rates of particles undergoing pyrolysis can be evaluated from a basic energy balance using the following equation.[35]

$$\frac{dT}{dt} = \frac{h_c(T_w - T)}{L \rho_p c_{p,p}} \quad (17)$$

While the heating rates decrease over time due to continuously increasing particle temperatures (T), determination of an initial heating rate has been recommended in the literature.[35] Our estimates show that the heating rate values were greater than 1000 °C/s at temperatures above 350 °C (see Figure S6, supplementary information) indicating that the fluidized bed reactor experiments reported here are consistent with flash pyrolysis.

To assess the fluidization characteristics of feed particles in the pyrolysis reactor, we estimated their minimum fluidization velocity (u_{mf}) and terminal velocity (u_t) using the correlations given below.[36, 37]

$$24.5Re_{p,mf}^2 + 1650Re_{p,mf} - Ar = 0 \quad (18)$$

where, $Re_{p,mf}$ is the particle Reynolds number at the minimum fluidization velocity ($=D_p u_{mf}\rho_g/\mu_g$) and Ar is the Archimedes number ($=\frac{\rho_p(\rho_p-\rho_g)D_p^3 g}{\mu_g^2}$)

$$u_t = D_p\left[\frac{4}{225}\frac{g(\rho_p-\rho_g)^2 g^2}{\mu\rho_g}\right]^{\frac{1}{3}} \quad (19)$$

Figure S7 (supplementary information) shows the temperature dependent changes in velocity of the carrier gas within the 1″ diameter reactor section and the larger diameter particle disengagement section (3″) along with u_t and u_{mf}. It can be seen that the velocity of the carrier gas in the particle disengagement chamber is much lower than the terminal velocity of the particle for the temperature range tested in this study. Thus, the reactor design and operating conditions allowed the fluidized particles to disengage or fall out from the carrier gas and re-enter the 1″ reactor section. The velocity of the carrier gas within the 1″ reactor section was calculated to be higher than the terminal velocity of the particle. This would allow particles to entrain in the carrier gas and stay fluidized in the reactor section.

3.3 Pyrolysis product yields

Figure 2 shows the weight percent (relative to the original feed mass) of the recovered liquids and char as well as the uncondensed gases for the pyrolysis experiments. The mass of uncondensed gases lost to the atmosphere was calculated by subtracting the mass of solid and liquid product from the feed mass (Equation 5). As expected, bio-oil production increased with an increase in reaction temperature from 250-610 °C. At 250 °C only 15 % of the initial feed mass was converted to liquid products, whereas, the bio-oil yield was much higher at 550 °C and 610 °C and nearly 70 % of the initial feed mass was recovered as liquid products. In addition to flash pyrolysis conditions, the high liquid products yield can be attributed to the packed-bed condenser used in the process. In some experiments, > 30 % of the bio-oil was recovered in the packed bed condenser (see inset to Figure 2). Additionally, the slight back pressure applied during the experiments (by simply throttling the product exit stream from the

condenser) likely contributed to high recovery of the bio-oils. The higher pressures (measured to be 20 psia in the reactor) cause an increase in bio-oil vapor concentrations in the condensers, which would improve the chances of aerosol coalescence to larger droplets.

Although bio-oil yields increased with reaction temperature, the conversion of solid to liquid was observed to be more temperature-sensitive below 460 °C (Figure 2). Nearly 85 % of the maximum bio-oil yield was achieved at or below 460 °C with an additional 15 % produced when the pyrolysis temperature was higher. Loss of solid mass was also correspondingly high over the temperature range 250-460 °C. Mass of char recovered remained approximately constant above this temperature (Figure 2). The components of soybean – protein, storage carbohydrates and triglycerides – are thermally labile below ~450 °C[27, 38, 39] and was likely the reason that most of the feed volatilization was observed at relatively low temperatures. In contrast, lignocellulose contains more thermally recalcitrant components, especially lignin,[40] and significant volatilization of feed continues at higher temperatures.[41, 42]

The uncondensed gases likely consisted of non-condensable gases such as H_2, CO_2, CO, and CH_4 that are produced during pyrolysis in addition to a small portion (if any) of unrecovered bio-oil vapors.[20] It can be noted that the mass fraction of uncondensed gases was lower at higher pyrolysis temperature (at 550 °C and 600 °C) when compared to uncondensed gases produced at 415 °C). This could be due to the faster kinetics at higher temperatures which would result in more concentrated vapors that were more easily condensed than the products from the lower temperatures

experiments. The low vapor residence time (τ_{vap}, Figure S5) also likely mitigated secondary reactions to non-condensable gases.

Figure 3 shows the yield (relative to feed mass) of aqueous- and oil-phases from pyrolysis at examined temperatures. The liquid products from pyrolysis at 250 °C and 280 °C consisted of a single aqueous phase. The production of water in oleaginous feeds at low temperatures, as observed in our experiments, could possibly be the result of release of bound moisture or from dehydration reactions of starch-like carbohydrates and/or protein.[43] Similar low temperature dehydration, referred to as "torrefaction", has been reported with lignocellulosic biomass.[44, 45] However, at 340 °C and higher, the liquid products were comprised of aqueous and oil phases that spontaneously separated. The oil phase content was observed to increase from 340 °C to 550 °C, however after 550 °C, oil phase content decreased, likely due to more extensive secondary vapor phase degradation. We also estimated the water content (measure by Karl-Fisher Titration) in the oil phase (inset to Figure 3) and observed that the water concentrations varied between 8-12 % (relative to the oil phase mass) and perhaps represent the water solubility limit of the hydrophobic phase.

3.4 Pyrolysis product analysis

Figure 4 shows the C (Figure 4a) and N (Figure 4b) mass fraction (relative to the feed) in bio-char, oil- and aqueous-phase at the investigated reaction temperatures. At the pyrolysis temperature of 250 °C, most of the C (>95 %) present in the original feed mass was recovered in the bio-char fraction due to low reactivity of biomass at this temperature. At 250 °C and 280 °C, the liquid product contained less than 4 % of feed C. At T>250 °C, a lower fraction of carbon in feed was recovered (in bio-char and liquid),

likely due to loss associated with non-condensable gases and uncondensed vapors. Somewhat surprisingly, the lowest C-recovery was observed at the intermediate temperature of 340 °C (~75 % of the feed C) while greater amounts of C (> 80 % of the feed C) was recovered during the higher temperature (415 °C and 550 °C). While it is unlikely that more non-condensable gases were produced at 340 °C than at higher temperatures, it is possible that a small fraction of the condensable bio-oils were not effectively captured (in condensers) during this intermediate temperature. As discussed previously, the rate of pyrolysis at lower temperatures was slow and resulted in a dilute vapor stream that was more difficult to capture in the condensers.

From Figure 4a, it can also be seen that the carbon content in the bio-char decreased (and corresponded to an increase in C recovered in the bio-oil) when pyrolysis temperatures were increased from 250 °C to 550 °C. This trend is expected due to greater thermal breakdown of biomass polymers to smaller molecules at higher temperatures. After pyrolysis at 550 °C, only 22 % of the feed C remained in the bio-char. At higher temperatures (>575 °C), C-content in bio-char is expected to remain unchanged due to formation of "fixed carbon". From Figure 4a, the typical carbon content in the aqueous phase was small. At temperatures where a distinct oil phase was formed (> 340 °C), < 5 % of the feed carbon partitioned into the aqueous phase.

Figure 4b shows the N mass (relative to the mass of the original feed) of the bio-char, oil- and aqueous-phase at reaction temperatures 250-610 °C. At 250 °C, most of the N remained in the char and little (if any) loss was observed, likely due to low reactivity at low temperature. At higher temperatures (≥ 280 °C), ~30 % of the initial N was lost into incondensable forms – most likely as ammonia.[11] At temperatures greater than 280 °C,

although the recovered N remained nearly constant, there appears to be a redistribution of N from char to bio-oil. This can be attributed to either a greater breakdown of protein (which forms smaller organic molecules), or reaction of the produced ammonia with products from pyrolysis of other biopolymers (carbohydrates and lipids) to form secondary N-compounds.[46-48] It is also possible that some ammonia remains dissolved in the aqueous phase since the organic acids (e.g. acetic acid) formed during pyrolysis reduce the pH of the organic phase which could allow ammonia to stay in solution as NH_4^+.

3.5 Lipid recovery from pyrolysis

To assess recovery of the biomass lipid fraction, the major lipid-derived compounds in bio-oil were identified by GC-MS and quantified using GC-FID (see example chromatograms in Figure S8 and S9, supplementary information). Figure 5 shows the most abundant lipid-derived components (relative to the initial feed mass) in bio-oil at the various pyrolysis temperatures tested. The lipid fraction of the bio-oil was mainly comprised of triglyceride, diglyceride, oleic acid, palmitic acid, and oleamide. During pyrolysis, the triglycerides exposed to elevated temperatures may breakdown into smaller molecules through thermal degradation or due to hydrolysis reactions with the water generated during pyrolysis.[49] However, the very short residence times inside the fluidized-bed reactor used for these experiments likely prevented more complete degradation of the triglycerides and diglycerides. Interestingly, monoglycerides were not detected among the products suggesting that these molecules are more reactive and possibly decomposed more rapidly than di- or tri- glycerides. Oleoamides were also

present in significant concentrations, possibly as a result of reaction of lipids with ammonia produced from protein degradation.[47, 50]

Pyrolysis at 415 °C or higher temperatures resulted in recovery of a majority of feed lipid in the liquid products. At 550 °C, as high as 90 % of the lipid content in feed was collected in bio-oil. Overall, high lipid recovery indicates that bio-oils from pyrolysis of oleaginous feedstocks retain the energy dense glycerides or their primary breakdown products (fatty acids).

3.6 Pyrolysis oil properties

The elemental composition, water content and higher heating values of the oil phase from flash pyrolysis at 550 °C is compared to *C. vulgaris*[15] and wood-derived[19] bio-oil and the results are listed in Table 2. One can observe that C- and H- content of bio-oil from soybean flake are higher than those of oil from wood, while the oxygen content is lower than of wood-derived oil. The decrease in the O-content of bio-oils from the oleaginous feedstocks (soybean and *C. vulgaris*) compared to those from wood (lignocellulose) is important because lower O-content improves the stability of bio-oil and decreases H_2 requirements for catalytic upgrading.[51] Moreover, the bio-oil from soybean has higher HHV (27 MJ/kg) due to higher contents of C and H and lower contents of O as well as lower acidity[5]. Water content of bio-oil from oleaginous biomass (bio-oil from soybean flake contains 10 %, and *C. vulgaris* has 16 % water) is also much less than wood-derived bio-oil. High water content bio-oil inhibits the hydrodeoxygenation (HDO) of bio-oil due to negative effects on activity, stability and selectivity of the commercial hydrotreating catalysts ($CoMo/Al_2O_3$ and $NiMo/ Al_2O_3$).[52] The N-content of bio-oils from soybean is higher than wood-derived bio-oil due to high

concentration of proteins in feedstock and is a drawback of thermochemical conversion of oleaginous feedstocks. However, it is possible to decrease the bio-oil N-content via hydrotreating.[53, 54]

4 Conclusions

A fluidized-bed flash pyrolysis apparatus was designed and constructed to convert oleaginous biomass into liquid fuels. A particle disengagement chamber incorporated into the reactor was effective at separating the particles (solid residue) from the carrier gas stream and prevented contamination of the recovered bio-oils. A unique dry ice packed-bed condenser, in series with traditional Allihn condensers, allowed for higher recoveries of bio-oil.

Soybean flake was used as the model oleaginous feed. Flash pyrolysis was carried out at temperatures 250-610 °C to and nearly 70 % bio-oil yields were obtained above 550 °C. The high liquid products yield can be attributed to the short vapor residence time (0.3-0.6 s) and the effective vapor condensation. At 550 °C, nearly 70 % of biomass carbon was recovered in bio-oil and bio-char. Also, at 550 °C, 90 % of the biomass lipids were collected in the bio-oil, which demonstrates that pyrolysis can effectively recover lipids from biomass. Bio-oil from oleaginous biomass contains higher C and H, but lower O compared to wood-derived bio-oil and thereby better heating value.

5 Acknowledgments

This project was supported by (1) the National Science Foundation through the Sustainable Energy Pathways Program (award# CHE-1230609) and (2) the US Department of Energy Bioenergy Technologies Office (award# DE-EE0005993).

6 References

1. Corma, A.; Huber, G. W.; Sauvanaud, L.; O'Connor, P., Processing biomass-derived oxygenates in the oil refinery: Catalytic cracking (FCC) reaction pathways and role of catalyst. *Journal of Catalysis* **2007,** *247* (2), 307-327.
2. Georgianna, D. R.; Mayfield, S. P., Exploiting diversity and synthetic biology for the production of algal biofuels. *Nature* **2012,** *488* (7411), 329-335.
3. Atabani, A. E.; Silitonga, A. S.; Ong, H. C.; Mahlia, T. M. I.; Masjuki, H. H.; Badruddin, I. A.; Fayaz, H., Non-edible vegetable oils: A critical evaluation of oil extraction, fatty acid compositions, biodiesel production, characteristics, engine performance and emissions production. *Renewable and Sustainable Energy Reviews* **2013,** *18*, 211-245.
4. Tripathi, M.; Mishra, A., Glucosinolates in animal nutrition: A review. *Animal Feed Science and Technology* **2007,** *132* (1), 1-27.
5. Boateng, A.; Mullen, C.; Goldberg, N., Producing stable pyrolysis liquids from the oil-seed presscakes of mustard family plants: Pennycress (Thlaspi arvense L.) and camelina (Camelina sativa). *Energy & Fuels* **2010,** *24* (12), 6624-6632.
6. Dose, H. L.; Eberle, C. A.; Forcella, F.; Gesch, R. W., Early planting dates maximize winter annual field pennycress (Thlaspi arvense L.) yield and oil content. *Industrial Crops and Products* **2017,** *97*, 477-483.
7. Hergert, G. W.; Margheim, J. F.; Pavlista, A. D.; Martin, D. L.; Isbell, T. A.; Supalla, R. J., Irrigation response and water productivity of deficit to fully irrigated spring camelina. *Agricultural Water Management* **2016,** *177*, 46-53.
8. Isbell, T. A., US effort in the development of new crops (Lesquerella, Pennycress Coriander and Cuphea). *OCL* **2009,** *16* (4-5-6), 205-210.
9. Brown, T. M.; Duan, P.; Savage, P. E., Hydrothermal Liquefaction and Gasification of Nannochloropsis sp. *Energy & Fuels* **2010,** *24* (6), 3639-3646.
10. Elliott, D. C.; Biller, P.; Ross, A. B.; Schmidt, A. J.; Jones, S. B., Hydrothermal liquefaction of biomass: Developments from batch to continuous process. *Bioresource Technology* **2015,** *178*, 147-156.
11. Wang, K.; Brown, R. C., Catalytic pyrolysis of microalgae for production of aromatics and ammonia. *Green Chemistry* **2013,** *15* (3), 675-681.
12. Huber, G. W.; Iborra, S.; Corma, A., Synthesis of transportation fuels from biomass: chemistry, catalysts, and engineering. *Chemical reviews* **2006,** *106* (9), 4044-4098.
13. Elliott, D. C., Review of recent reports on process technology for thermochemical conversion of whole algae to liquid fuels. *Algal Research* **2016,** *13*, 255-263.
14. Valdez, P. J.; Nelson, M. C.; Wang, H. Y.; Lin, X. N.; Savage, P. E., Hydrothermal liquefaction of Nannochloropsis sp.: Systematic study of process variables and analysis of the product fractions. *Biomass and Bioenergy* **2013,** *46* (0), 317-331.
15. Wang, K.; Brown, R. C.; Homsy, S.; Martinez, L.; Sidhu, S. S., Fast pyrolysis of microalgae remnants in a fluidized bed reactor for bio-oil and biochar production. *Bioresource Technology* **2013,** *127*, 494-499.
16. Babu, B. V., Biomass pyrolysis: A state-of-the-art review. *Biofuels, Bioproducts and Biorefining* **2008,** *2* (5), 393-414.

17. Stevens, C.; Brown, R. C., *Thermochemical processing of biomass: conversion into fuels, chemicals and power*. John Wiley & Sons: 2011.
18. Bridgwater, A. V.; Peacocke, G. V. C., Fast pyrolysis processes for biomass. *Renewable and Sustainable Energy Reviews* **2000,** *4* (1), 1-73.
19. Bridgwater, A. V., Review of fast pyrolysis of biomass and product upgrading. *Biomass and bioenergy* **2012,** *38*, 68-94.
20. Horne, P. A.; Williams, P. T., Influence of temperature on the products from the flash pyrolysis of biomass. *Fuel* **1996,** *75* (9), 1051-1059.
21. Linstrom, P. J.; Mallard, W. G., *NIST Chemistry WebBook, NIST Standard Reference Database Number 69*. National Institute of Standards and Technology: Gaithersburg MD, 20899, retrieved May 2, 2017.
22. Levenspiel, O., *Engineering Flow and Heat Exchange*. Springer: 1998.
23. Perry's, R.; Chilton, C.; Kirkpatrick, S., Chemical engineers handbook. *Chemical engineers handbook* **1999**.
24. Bligh, E. G.; Dyer, W. J., A rapid method of total lipid extraction and purification. *Canadian journal of biochemistry and physiology* **1959,** *37* (8), 911-917.
25. Dong, F. M.; Hardy, R. W.; Haard, N. F.; Barrows, F. T.; Rasco, B. A.; Fairgrieve, W. T.; Forster, I. P., Chemical composition and protein digestibility of poultry by-product meals for salmonid diets. *Aquaculture* **1993,** *116* (2), 149-158.
26. Friedl, A.; Padouvas, E.; Rotter, H.; Varmuza, K., Prediction of heating values of biomass fuel from elemental composition. *Analytica Chimica Acta* **2005,** *544* (1–2), 191-198.
27. Maddi, B.; Viamajala, S.; Varanasi, S., Comparative study of pyrolysis of algal biomass from natural lake blooms with lignocellulosic biomass. *Bioresource Technology* **2011,** *102* (23), 11018-11026.
28. Agblevor, F. A.; Besler, S., Inorganic Compounds in Biomass Feedstocks. 1. Effect on the Quality of Fast Pyrolysis Oils. *Energy & Fuels* **1996,** *10* (2), 293-298.
29. Ranz, W. E.; Marshall, W. R., Evaporation from Drops. *Chemical Engineering Progress* **1952,** *48*, 173-180.
30. Eriksson, M.; Golriz, M. R., Radiation heat transfer in circulating fluidized bed combustors. *International Journal of Thermal Sciences* **2005,** *44* (4), 399-409.
31. Pyle, D. L.; Zaror, C. A., Heat transfer and kinetics in the low temperature pyrolysis of solids. *Chemical Engineering Science* **1984,** *39* (1), 147-158.
32. Deshpande, S. D.; Bal, S.; Ojha, T. P., Bulk thermal conductivity and diffusivity of soybean. *Journal of Food Processing and Preservation* **1996,** *20* (3), 177-189.
33. Jayas, D. S.; Cenkowski, S., Chapter 27: Grain Property Values and Their Measurement. In *Handbook of Industrial Drying*, 4th ed.; Mujumdar, A. S., Ed. CRC Press: Boca Raton, FL, 2014.
34. Deshpande, S. D.; Bal, S., Specific heat of soybean. *Journal of Food Process Engineering* **1999,** *22* (6), 469-477.
35. Lédé, J., Biomass Pyrolysis: Comments on Some Sources of Confusions in the Definitions of Temperatures and Heating Rates. *Energies* **2010,** *3* (4), 886.
36. Fueyo, N.; Dopazo, C., Fluidization fundamentals. In *Pressurized Fluidized Bed Combustion*, Cuenca, M. A.; Anthony, E. J., Eds. Springer Netherlands: Dordrecht, 1995; pp 38-79.

37. Wen, C. Y.; Yu, Y. H., Mechanics of Fluidization. *Chemical engineering progress symposium series* **1966,** *162*, 100-111.
38. Maddi, B. Pyrolysis Strategies for Effective Utilization of Lignocellulosic and Algal Biomass. Ph.D. Thesis, University of Toledo, Toledo, Ohio, 2014.
39. Shirazi, Y.; Viamajala, S.; Varanasi, S., High-yield production of fuel-and oleochemical-precursors from triacylglycerols in a novel continuous-flow pyrolysis reactor. *Applied Energy* **2016,** *179*, 755-764.
40. Kawamoto, H., Lignin pyrolysis reactions. *Journal of Wood Science* **2017,** *63* (2), 117-132.
41. Westerhof, R. J. M.; Brilman, D. W. F.; van Swaaij, W. P. M.; Kersten, S. R. A., Effect of Temperature in Fluidized Bed Fast Pyrolysis of Biomass: Oil Quality Assessment in Test Units. *Industrial & Engineering Chemistry Research* **2010,** *49* (3), 1160-1168.
42. Garcia-Perez, M.; Wang, X. S.; Shen, J.; Rhodes, M. J.; Tian, F.; Lee, W.-J.; Wu, H.; Li, C.-Z., Fast Pyrolysis of Oil Mallee Woody Biomass: Effect of Temperature on the Yield and Quality of Pyrolysis Products. *Industrial & Engineering Chemistry Research* **2008,** *47* (6), 1846-1854.
43. Wu, K.-T.; Tsai, C.-J.; Chen, C.-S.; Chen, H.-W., The characteristics of torrefied microalgae. *Applied Energy* **2012,** *100*, 52-57.
44. Tumuluru, J. S.; Sokhansanj, S.; Wright, C. T.; Hess, J. R.; Boardman, R. D. In *A review on biomass torrefaction process and product properties*, S-1041 Symposium on Thermochemical Conversion, Oklahoma State University, Stillwater, 2011.
45. Bridgeman, T. G.; Jones, J. M.; Shield, I.; Williams, P. T., Torrefaction of reed canary grass, wheat straw and willow to enhance solid fuel qualities and combustion properties. *Fuel* **2008,** *87* (6), 844-856.
46. Xu, L.; Yao, Q.; Deng, J.; Han, Z.; Zhang, Y.; Fu, Y.; Huber, G. W.; Guo, Q., Renewable N-heterocycles production by thermocatalytic conversion and ammonization of biomass over ZSM-5. *ACS Sustainable Chemistry & Engineering* **2015,** *3* (11), 2890-2899.
47. Mekki-Berrada, A.; Bennici, S.; Gillet, J.; Couturier, J.; Dubois, J.; Auroux, A., Fatty acid methyl esters into nitriles: acid–base properties for enhanced catalysts. *Journal of catalysis* **2013,** *306*, 30-37.
48. Xu, L.; Yao, Q.; Han, Z.; Zhang, Y.; Fu, Y., Producing Pyridines via Thermocatalytic Conversion and Ammonization of Waste Polylactic Acid over Zeolites. *ACS Sustainable Chemistry & Engineering* **2016,** *4* (3), 1115-1122.
49. Crossley, A.; Heyes, T. D.; Hudson, B. J. F., The effect of heat on pure triglycerides. *J Am Oil Chem Soc* **1962,** *39* (1), 9-14.
50. Mekki□Berrada, A.; Bennici, S.; Gillet, J. P.; Couturier, J. L.; Dubois, J. L.; Auroux, A., Ammoniation–Dehydration of Fatty Acids into Nitriles: Heterogeneous or Homogeneous Catalysis? *ChemSusChem* **2013,** *6* (8), 1478-1489.
51. Mullen, C. A.; Boateng, A. A., Production and analysis of fast pyrolysis oils from proteinaceous biomass. *BioEnergy Research* **2011,** *4* (4), 303-311.
52. Şenol, O. İ.; Viljava, T. R.; Krause, A. O. I., Hydrodeoxygenation of aliphatic esters on sulphided NiMo/γ-Al2O3 and CoMo/γ-Al2O3 catalyst: The effect of water. *Catalysis Today* **2005,** *106* (1–4), 186-189.

53. Perot, G., The reactions involved in hydrodenitrogenation. *Catalysis Today* **1991,** *10* (4), 447-472.
54. Izhar, S.; Uehara, S.; Yoshida, N.; Yamamoto, Y.; Morioka, T.; Nagai, M., Hydrodenitrogenation of fast pyrolysis bio-oil derived from sewage sludge on NiMo/Al2O3 sulfide catalyst. *Fuel Processing Technology* **2012,** *101*, 10-15.

7 Figures

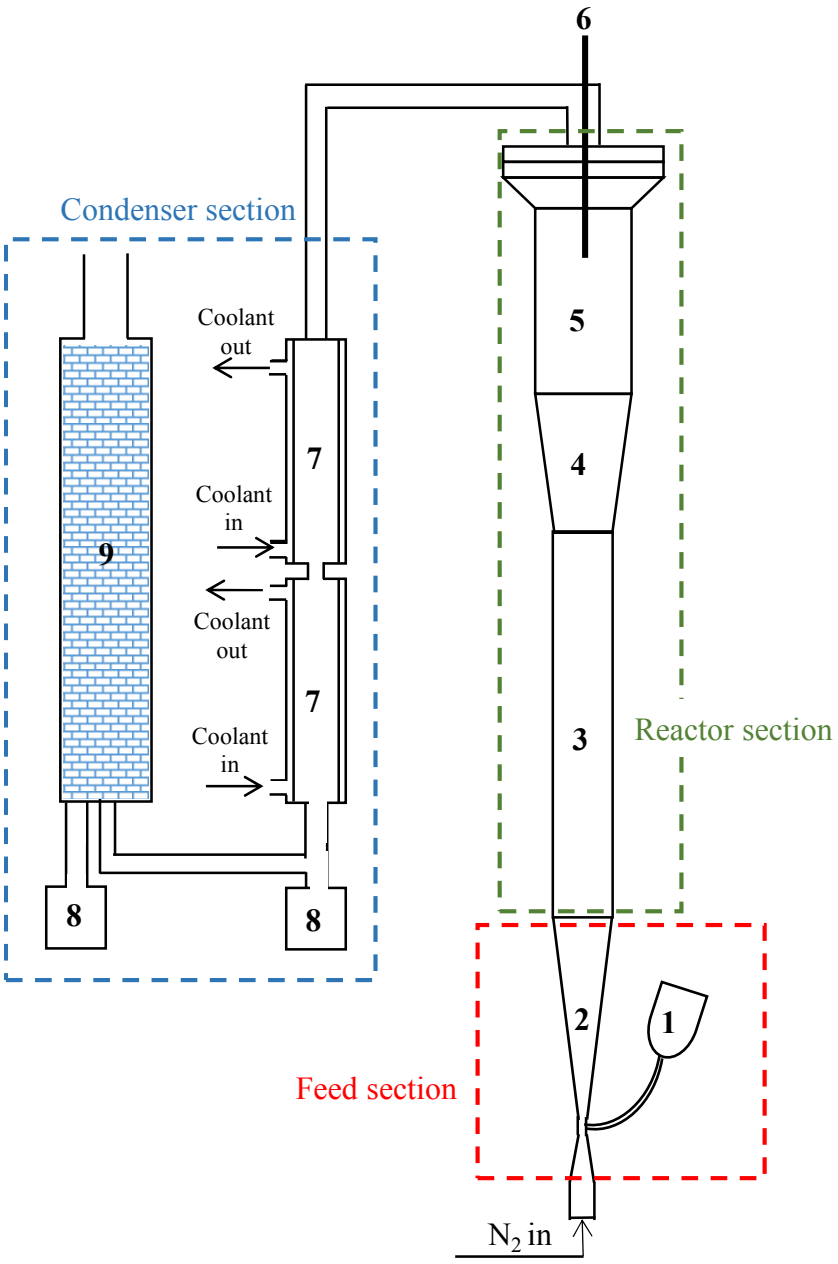

Figure 1. Schematic diagram of flash fluidized-bed pyrolysis. The dashed blocks represents feed, reactor and condenser sections. 1: feed hopper, 2: venture, 3: 1" reactor, 4: expander, 5: 3" disengagement chamber, 6: thermocouple, 7: Allihn condensers, 8: bio-oil liquid trap, 9: dry ice packed-bed condenser. The scaled drawing of the reactor with dimensions is shown in Figure S1 (supplementary information)

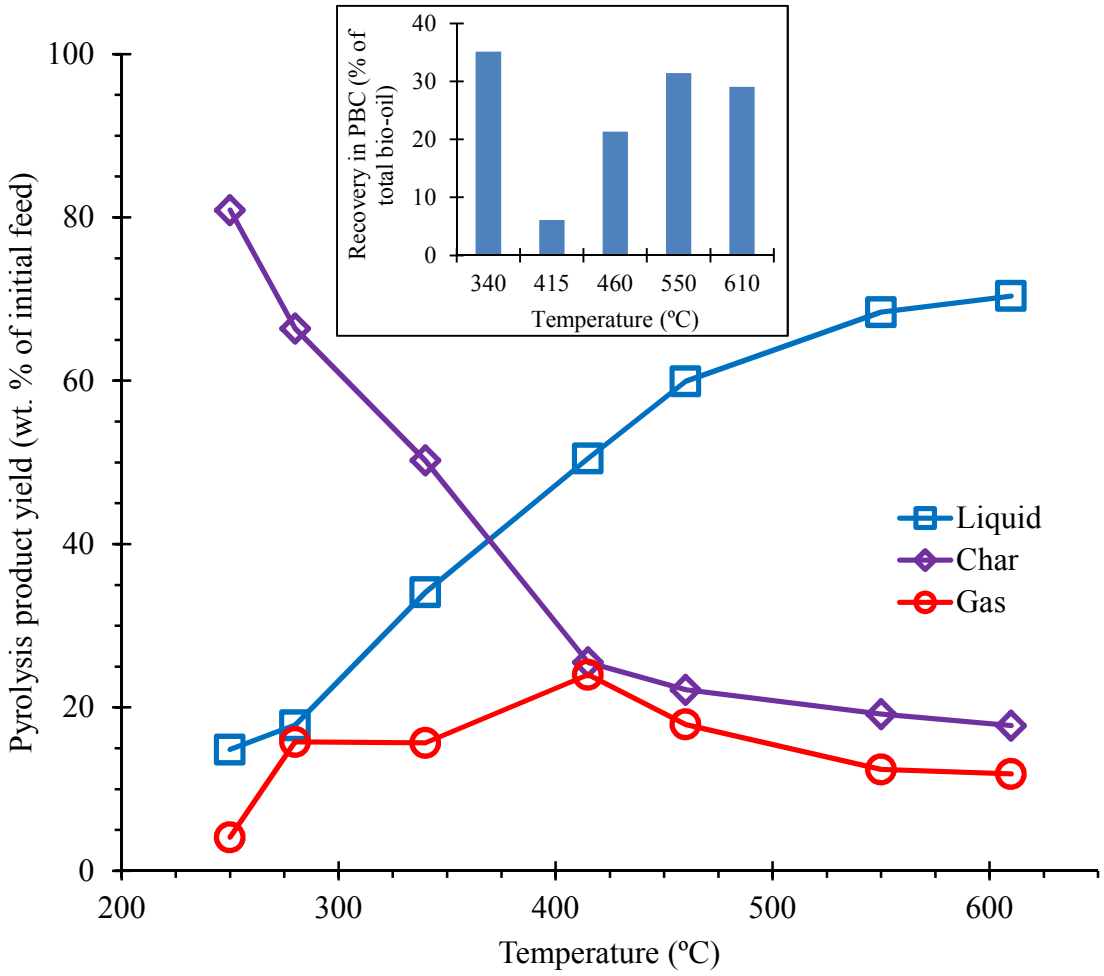

Figure 2. Relative weights of liquid, char and gaseous products from flash pyrolysis. The values are reported relative to the initial feed mass. Inset shows bio-oil recovered in the packed bed condenser (PBC) as a fraction of total bio-oil recovered.

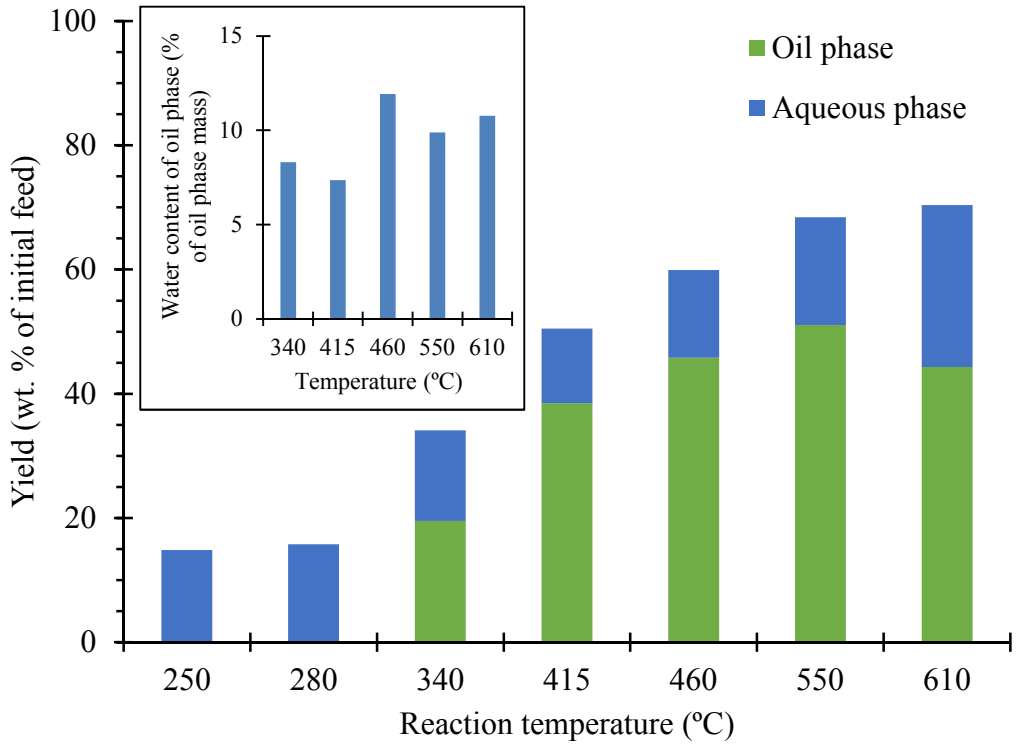

Figure 3. Oil- and aqueous-phase bio-oil yields (reported as a fraction of the initial feed mass) at tested pyrolysis temperatures. Inset shows water content of oil phase.

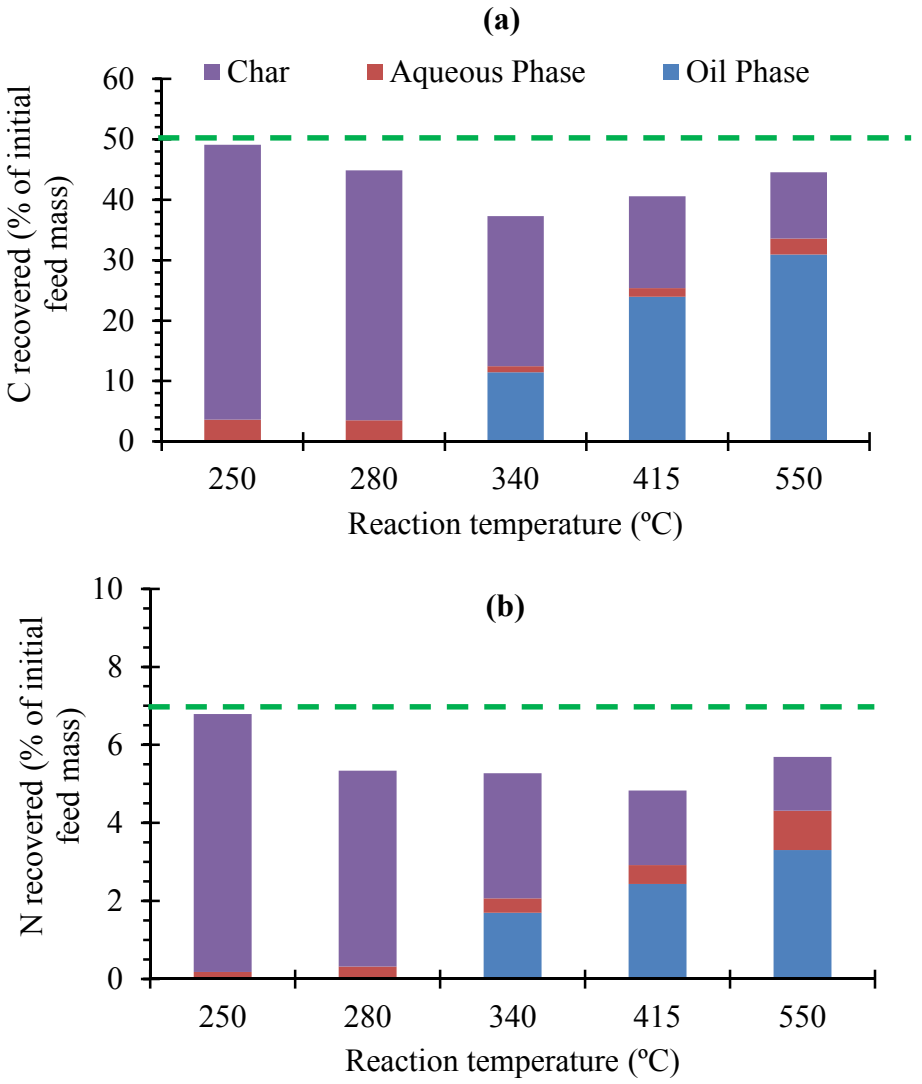

Figure 4. Recovery of (a) carbon and (b) nitrogen in char, aqueous and oil phase. The green dashed lines represents the wt. % of C and N in the feedstock.

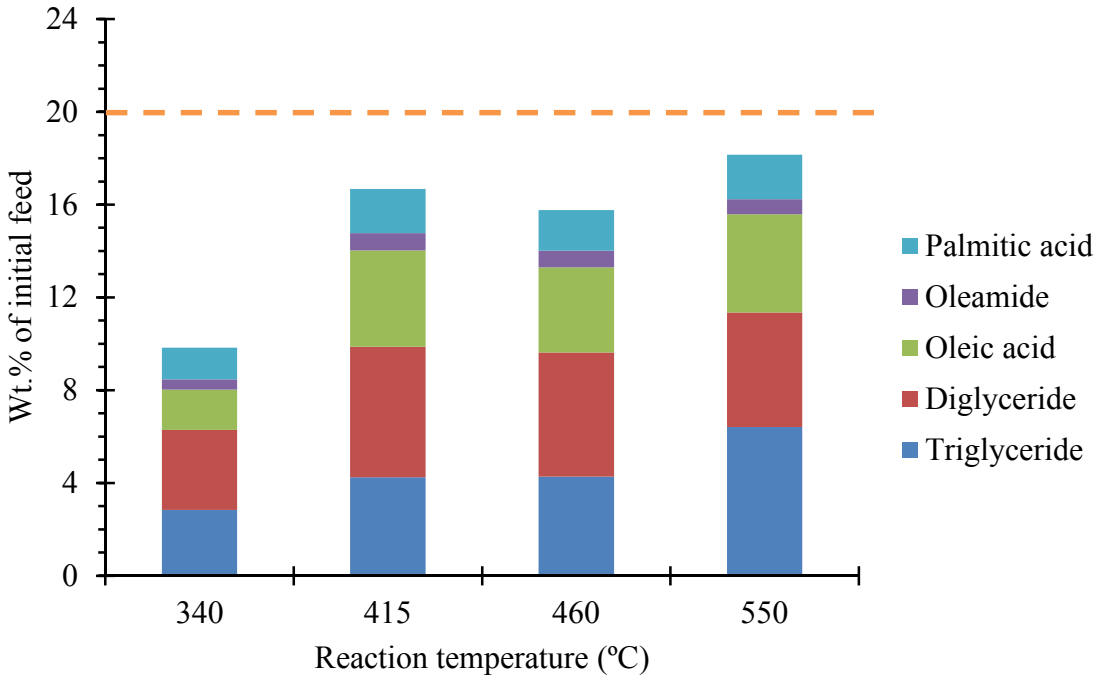

Figure 5. Relative mass of the major lipid-derived products recovered in bio-oil from flash pyrolysis. The dashed line represents lipid content of feedstock.

8 Tables

Table 1. Compositional, proximate and ultimate analysis. Carbohydrates include cellulose hemicellulose in the woodchips and starch in soybean and *C. vulgaris*. Woodchips consisted of lignin instead of lipid. Mass fraction of O was calculated by difference.

Properties	Feedstock		
Compositional analysis (wt. %)	Soybean flake	*C. vulgaris*[a]	Woodchips[b]
Lipid	20	15.7	–[#]
Carbohydrate	25.9	21.0	62.2
Protein	43.8	41.5	0.6
Proximate analysis [*$] (wt. %)			
Volatiles	75.4	71	77.6
Fixed carbon	19.8	12.4	20.6
Ash	4.8	16.6	1.8
Ultimate analysis [*] (wt. %)			
C	51.0	42.5	52.9
H	8.0	6.8	7.1
N	7.0	6.6	0.1
O	29.6	28.0	37.9
C/O	2.3	2.0	1.9
H/C	1.9	1.9	1.6
HHV (MJ/kg)	23.2	16.8	21.7

[#]: Lignin equal to 23.7 %
[*]: Dry basis
[$]: Values are normalized based on biomass moisture content; soybean flake: 5.9 %; *C. vulgaris*: 6.2 %; woodchips: 15.1 %
[a]: Data taken from reference [15]
[b]: Data taken from reference [27]

Table 2. Elemental analysis of pyrolysis bio-oil from present study and literature.

Properties	Feedstock		
	Soybean	*C. vulgaris*[a]	Wood[b]
Water (wt. %)	9.9	15.9	25
C (wt. %)	60.6	51.4	56
H (wt. %)	8.4	8.3	6
N (wt. %)	6.5	12.8	<0.1
O (wt. %)	24.5	27.5	38
H/C	1.7	1.9	1.3
C/O	3.3	2.5	2.0
HHV (MJ/kg)	27.5	24.6	17

[a]: Data taken from reference [15]
[b]: Data taken from reference [19]